Chapter 23
Computational Fluid Dynamic Analysis of Amphibious Vehicle

H. Jaouad, P. Vikram, E. Balasubramanian and G. Surendar

Abstract Development of unmanned amphibious vehicle for diverse applications including monitoring of oil-spills, military border and water quality measurement in remote water bodies are in the rise. These vehicles suffer for its stability and endurance due to the effect of drag in varied wind conditions. The present work focused on minimizing the drag and improving the aerodynamic performance characteristics. The computational fluid dynamic analysis is performed through considering various turbulent models such as k-ω, k-ε and SST k-ω (shear stress transport) to estimate the co-efficient of drag of the designed amphibious vehicle. Static analysis is performed through varying the angle of attack (AoA) from 0^0 to 10^0 under relative airspeed of 5, 8.3 and 10 m/sec. The velocity, pressure and turbulent kinetic energy contours predicted the streamline of air flow around the vehicle and instability regions.

Keywords Amphibious UAV · CFD · RANS model · Drag · Blunt body

23.1 Introduction

Unmanned aerial vehicles (UAVs) are predominantly used in diverse applications [1, 2] including precision agriculture, environmental monitoring, aerial photography, search and rescue, surveillance and reconnaissance, power line and telecom

H. Jaouad
Polytech Orleans, Orleans, France
e-mail: jaouad.hajjaji@gmail.com

P. Vikram · E. Balasubramanian (✉) · G. Surendar
Vel Tech Rangarajan Dr. Sagunthala R & D Institute of Science and Technology, Chennai, India
e-mail: esak.bala@gmail.com

P. Vikram
e-mail: vikram.veeran@gmail.com

G. Surendar
e-mail: suren.ganesh.2007@gmail.com

tower inspections. However, usage of UAVs in water quality monitoring and collection of water samples in remote water bodies are scarce. Especially, the design of amphibian characteristics UAVs which can fly, land and glide along the water surface imposing a lot of challenges in terms of control in flight transition, selection of materials, propulsion, energy consumption and payload capacity [3]. In addition, other factors such as durability, reliability, safety and minimal cost are utmost important for industrial demand and customer requirement. There are few floating UAVs which have been developed and commercialized in the market [4]. However, integrating the characteristics of multirotor and hovercraft systems are not being explored in the literature. These vehicles are aimed to cover large areas of water bodies in a short span of time. Unlike other floating vehicles, due to the principle of hovercraft [5], the friction between the vehicle and water surface is avoided and thereby a huge amount of energy is saved. The vertical take-off and landing ability of vehicle can position the vehicle in precise water locations across rivers, ponds and other water bodies to collect water samples. One of the aerodynamic parameters influencing endurance of amphibious vehicle is a drag. There are few studies have been conducted to calculate the drag of fixed-wing and rotary-wing vehicles. Sitaraman and Baeder [6] carried out aerodynamic analysis of quadrotor using Navier–Stokes equation and wake interactions are studied. Steijl et al. [7] studied rotor and fuselage interaction using CFD analysis using a sliding plane technique. The turbulent flow characteristics [8] during inviscid and viscid fluids are simulated in CFD to analyse the behaviour of shrouds of the multirotor system. Biava et al. [9] examined the aerodynamic behaviour of the helicopter through CFD and experimental studies. Kusyumov et al. [10] carried out a CFD analysis of ANSAT helicopter to determine lift and drag forces in viscous flow conditions. Yoon et al. analysed [11] the flow distribution over fixed-wing aerofoil through varied AoA and co-efficient of drag and lift are obtained. Abudarag et al. [12] studied the flow separation between rotor and fuselage using CFD and turbulent flow characteristics are examined. The present work concentrates on performing CFD studies on various turbulent models [13–15] such as k-ω, k-ε and SST k-ω for determining the co-efficient of drag under various AoA and relative airspeed conditions.

23.2   Modelling

The conceptualization amphibian model is designed by inculcating the principles of the quadrotor and hovercraft. This vehicle is capable of flying in the air as a multirotor system and hovering in the water like a hovercraft. After many design iterations, the amphibious UAV model has 1.2 m of length 0.6 m of width and 0.48 m of height is finalized to carry a payload of 7 kg. Propeller has 0.7 m of diameter and 0.182 m of the pitch to generate 10 kg of thrust force. In order to reduce the computational effort, the model is scaled down to a factor of 1:0.25. Also, to maintain the Reynolds number with reference to the prototype, velocity is increased four times and various wind speed conditions are accounted for simulation studies (Fig. 23.1).
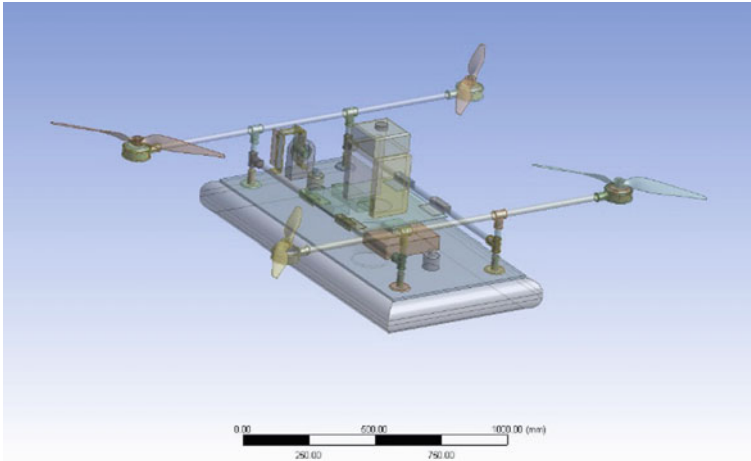
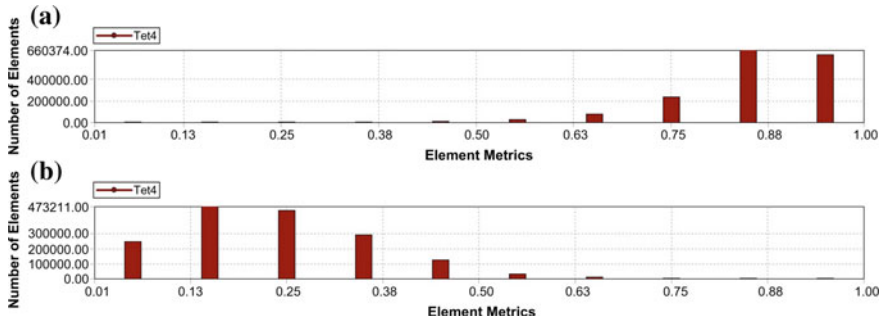**Fig. 23.1** Conceptualized model of amphibious vehicle

Fig. 23.2 **a** Orthogonality of elements. **b** Skewness of elements

The scaled down amphibian structure is meshed with tetrahedron element using ICEM tool. Grid quality is verified with orthogonality (Fig. 23.2a) and skewness and checks (Fig. 23.2b). The average mesh size of the element is maintained as 5,00,000 and 6,00,000 elements.

23.3 Computational Fluid Dynamic Analysis

The turbulent flows are computed by solving Reynolds-averaged Navier–Stokes equations (RANS). Shear stress transport (SST) k-ω model given in Eqs. (23.1) and (23.2) is utilized to calculate the near-wall flow characteristics using a blending function. It also estimates the flow properties away from the wall surface. In the SST k-ω model, a damped cross-diffusion term is used to determine the turbulent shear

stress through modifying the turbulent viscosity which ensures the selected model is more accurate and reliable for diverse flow fields

Kinematic eddy viscosity

$$v_T = \frac{\alpha_1 k}{\max(\alpha_1 k, SF_2)} \tag{23.1}$$

Turbulent kinetic energy

$$\frac{\partial k}{\partial t} + U_j \frac{\partial k}{\partial x_j} = P_k - \beta^* k\omega + \frac{\partial}{\partial x_j}\left[(v + \sigma_k v_T)\frac{\partial k}{\partial x_j}\right] \tag{23.2}$$

CFD analysis is performed through varying the AoA under various relative air velocity conditions. Simulation studies are conducted [10] for the following three cases of velocity conditions.

Case 1: 5 m/s
CFD analysis is performed through varying the angle of attack (AoA) from 0^0–10^0 at the relative airspeed of 5 m/sec (Fig. 23.3). During 0^0 AoA, high reverse flow region occurs behind the water sampler module region. While increasing the AoA, the velocity regimes are streamlined and at 8^0 AoA reverse flow around the amphibious vehicle is streamlined which reduces drag. Further, an increase of AoA leads to the formation of the turbulent region at the rear of the vehicle that may cause an increase of the drag. It is evident from pressure contours of varied AoA, up to 8^0, there is a decrease in the trend of pressure and a further increase of AoA causes an increase in pressure in the upstream region and there is a possibility of instability vehicle. Also, above 8^0 of AoA, the intensity of turbulence is increased which may lead to vibration and unable to control the vehicle in the desired path.

Case 2: 8.3 m/s
A similar phenomenon is observed as in the case of 5 m/s. However, the intensity of velocity and pressure is quite high as compared to 5 m/s (Fig. 23.4).

Case 3: 10 m/s
The intensity of turbulence is increased at high relative airspeed which can be seen in Fig. 23.5. For various wind speed conditions and AoA, the co-efficient of drag and lift is estimated which is given in Table 23.1. It is observed that increase in AoA and wind speed causes an increase in drag and a decrease in lift. The lift-to-drag ratio for the wind speed of 8.3 m/s given in Table 23.2 reveals that at 8^0 AoA, high amount of lift is generated with minimal drag.

CFD analysis is performed for half- and full-scale model to validate the results obtained through simulation. It is evident from Table 23.3 that the minimal error is obtained and hence half-scale model can be utilized for CFD analysis to overcome the computational burden and save a lot of time.

For various turbulent models such as k-ω, k-ε and SST k-ω, CFD analysis is performed and corresponding drag force is determined. Since, k-ω is considered as a standard model to measure the drag force, with reference to that error is calculated.
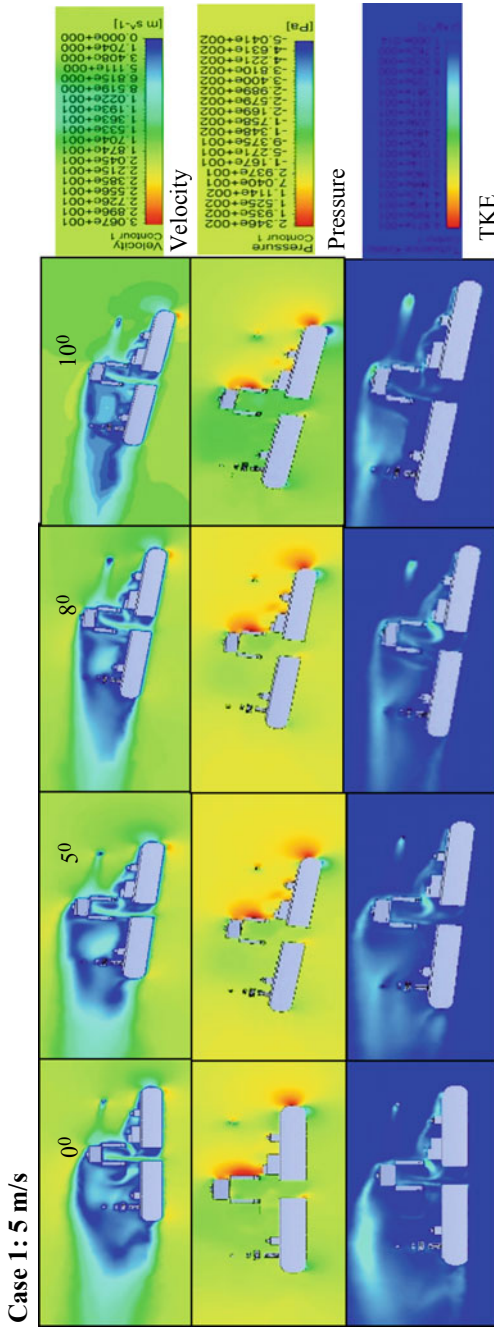
Fig. 23.3 Velocity, pressure and turbulence kinetic energy contours at 5 m/s

Case 2: 8.3 m/s
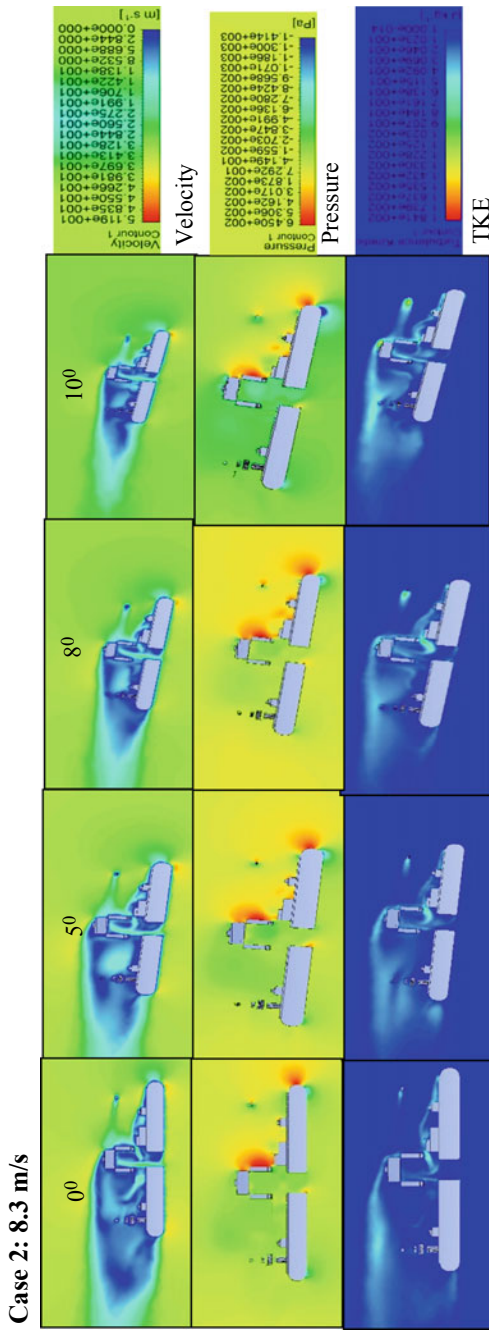
Fig. 23.4 Velocity, pressure and turbulence kinetic energy (TKE) contours at 8.3 m/s
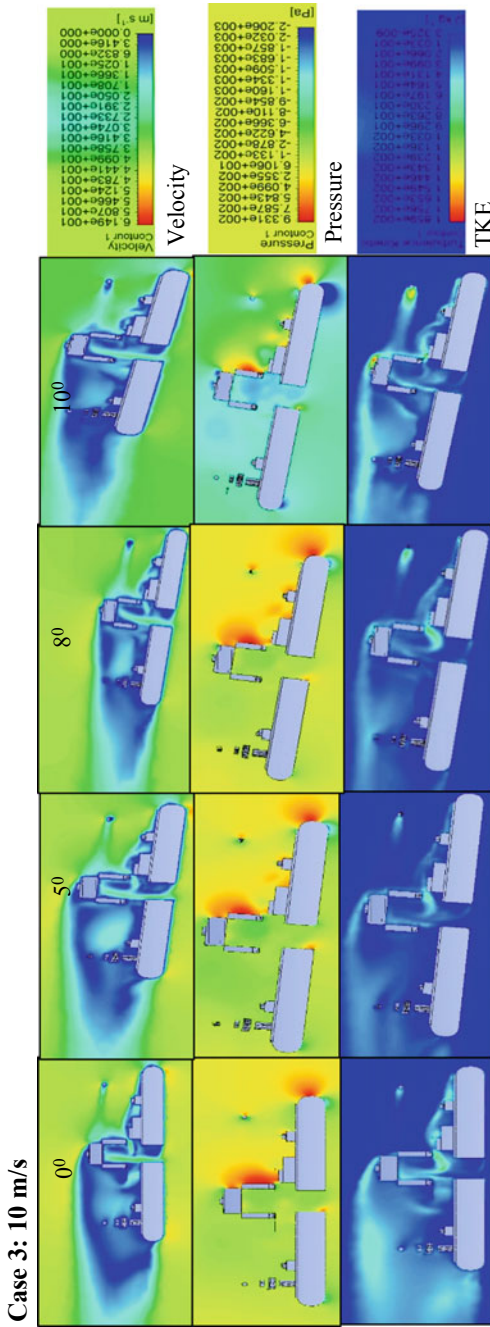
Fig. 23.5 Velocity, pressure and turbulence kinetic energy (TKE) contours at 10 m/s

Table 23.1 Estimation of drag for various AoA under different wind speed conditions

Wind speed (m/s)	Parameters	Angle of attack			
		0°	5°	8°	10°
5.0	C_D	0.489	0.346	0.364	0.382
	C_L	0.165	0.142	0.269	0.285
	Drag	1.32	1.27	1.327	1.529
8.3	C_D	0.489	0.352	0.364	0.382
	C_L	0.165	0.156	0.272	0.249
	Drag	3.639	3.582	3.654	4.213
10.0	C_D	0.489	0.349	0.367	0.379
	C_L	0.201	0.147	0.28	0.229
	Drag	5.28	5.157	5.358	6.059

Table 23.2 Lift-to-drag ratio at 8.3 m/sec

AoA (deg)	Drag (N)	Lift (N)	L/D ratio
0	3.639	1.265	0.348
5	3.582	1.591	0.444
8	3.654	2.731	0.747
10	4.213	2.745	0.652

Table 23.3 Comparison of drag for full- and half-scale amphibious model

| AoA (deg)	Relative velocity (m/s)	Drag for full model (N)	Drag for the half model (N)	Error
5	5	2.617	1.278	0.061
	8.3	7.217	3.582	0.051
8	5	2.486	1.327	−0.168
	8.3	6.948	3.654	−0.36

Minimum error is obtained for these models which are given in Table 23.4, and they can be used to calculate the drag force.

At 8.3 m/sec two extreme AoA of conditions (0^0 and 8^0), the velocity streamline pattern is shown in Figs. 23.6 and 23.7. It is observed that there is a severe recirculation zone at 0^0 and at 8^0 AoA. It is completely minimized. Hence, at 8^0 AoA, the amphibious vehicle experiences minimal drag.
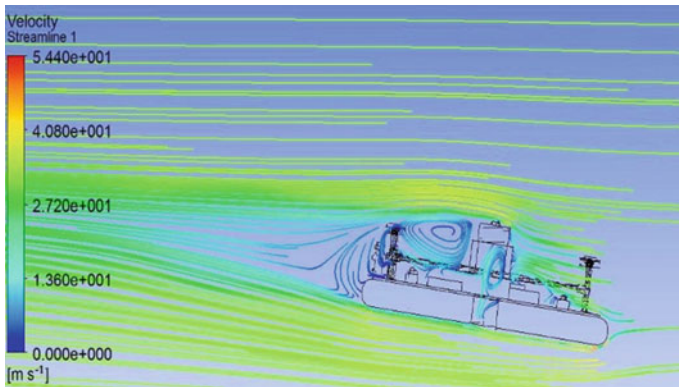
Table 23.4   Computation of drag using various turbulent models

AoA (deg)	Relative velocity (m/s)	Drag (N) (k-ω model)	Drag (N) (k-ε model)	Drag (N) (SST k-ω model)	Error (k-ω/SST k-ω)	Error (k-ω/k-ε)
5	5	3.615	3.639	3.560	−0.055	−0.024
	8.3	3.582	3.577	3.593	0.011	0.005
8	5	3.654	3.743	3.701	0.047	−0.089
	8.3	4.213	4.298	4.312	0.099	−0.085
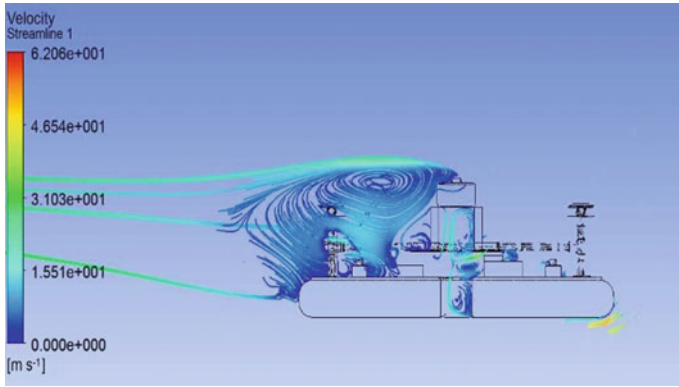
Fig. 23.6   Velocity Streamline 8.3 m/s at 0^0 AoA

Fig. 23.7   Velocity Streamline 8.3 m/s at 8^0 AoA

23.4 Conclusion

CFD analysis is performed for the designed amphibian structure through varying the AoA from 0^0 to 10^0 under different wind speed conditions (5, 8.3 and 10 m/s) and corresponding co-efficient of drag and lift force is calculated. At 8.3 m/s and 8^0 AoA, the maximum L/D ratio is obtained in comparison with other operating conditions and hence it is well suited for cruise flight. In addition, CFD studies are conducted for half- and full-scale amphibious models and drag force is calculated. It is evident that the error between these models is minimal and hence the half-scale model can be further utilized to perform CFD analysis. Comparative evaluation of various turbulent models such as k-ω, k-ε and SST k-ω suggested that error between standard k-ω and other models is minimum and hence they can be also used for dynamic analysis.

References

1. Valavanis, K. P., Vachtsevanos, G. J.: Handbook of unmanned aerial vehicles. Springer (2014)
2. Hassanalian, M., Abdelkefi, A.: Classifications, applications, and design challenges of drones: a review. Prog. Aerosp. Sci. **91**, 99–131 (2017)
3. Pisanich, G., Morris, S.: Fielding an amphibious UAV—development, results, and lessons learned. Digital Avionics Systems Conference, vol. 2, pp. 8C4–8C4 (2002)
4. Boxerbaum, A.S., Werk, P., Quinn, R.D., Vaidyanathan, R.: Design of an autonomous amphibious robot for surf zone operation: Part I mechanical design for multi-mode mobility. In Advanced Intelligent Mechatronics Proceedings, IEEE/ASME International Conference, pp. 1459–1464 (2005)
5. Amyot, J.R.: Hovercraft technology, economics and applications, vol. 11. North Holland. (2013)
6. Sitaraman, J., Baeder, J.: Analysis of quad-tiltrotor blade aerodynamic loads using coupled CFD/free wake analysis. In 20th AIAA Applied Aerodynamics Conference, p. 2813. (2002)
7. Steijl, R., Barakos, G., Badcock, K.: CFD analysis of rotor-fuselage aerodynamics based on a sliding mesh algorithm. (2007)
8. Grondin, G., Thipyopas, C., Moschetta, J.M.: Aerodynhamic analysis of a multi-mission short shrouded coaxial UAV: part III-CFD for hovering flight. In 28th AIAA Applied Aerodynamics Conference, p. 5073. (2010)
9. Biava, M., Khier, W., Vigevano, L.: CFD prediction of air flow past a full helicopter configuration. Aerosp. Sci. Technol. **19**(1), 3–18 (2012)
10. Kusyumov, A., Mikhailov, S.A., Garipov, A.O., Nikolaev, E.I., Barakos, G.: CFD simulation of fuselage aerodynamics of the ANSAT helicopter prototype. Trans. Control Mech. Syst. **1**(7), 318–324 (2015)
11. Yoon, S., Lee, H. C., Pulliam, T.H.: Computational analysis of multi-rotor flows. In 54th AIAA Aerospace Sciences Meeting, p. 0812. (2016)
12. Abudarag, S., Yagoub, R., Elfatih, H., Filipovic, Z.: Computational analysis of unmanned aerial vehicle (UAV). In AIP Conference Proceedings, vol. 1798, no. 1, p. 020001. AIP Publishing (2017, January)
13. Lesieur, M.: Turbulence in fluids: stochastic and numerical modelling. Nijhoff, Boston, MA (1987)

14. Versteeg, H.K., Malalasekera, W.: An introduction to computational fluid dynamics: the finite volume method. Pearson Education. (2007)
15. Ferziger, J.H., Peric, M.: Computational methods for fluid dynamics. Springer Science & Business Media. (2012)